JOURNAL OF SOLID STATE CHEMISTRY 105, 434–443 (1993)

Structural Origin of the Semiconducting Properties of $Sb_4Mo_{20}O_{62}$

ENRIC CANADELL

Laboratoire de Chimie Théorique, Université de Paris-Sud, 91405 Orsay Cedex, France

MICHEL EVAIN AND MARCEL GANNE

Laboratorire de Chimie des Solides, Institut des Materiaux de Nantes, Université de Nantes, 44072 Nantes Cedex, France

AND MYUNG-HWAN WHANGBO

Department of Chemistry, North Carolina State University, Raleigh, North Carolina 27695-8204

Received October 26, 1992; in revised form January 15, 1993; accepted January 19, 1993

The origin of the semiconducting properties of the molybdenum bronze $Sb_4Mo_{20}O_{62}$ was examined by performing tight-binding electronic band structure calculations. Our calculations show a band gap at the Fermi level, so that $Sb_4Mo_{20}O_{62}$ is not a Mott insulator but a regular semiconductor. Analysis of the low-lying t_{2g}-block bands reveals that the band gap originates from the O–Mo ··· O alternations in the six different types of MoO_6 octahedra present in $Sb_4Mo_{20}O_{62}$, and the conductivity of this bronze is one-dimensional despite its three-dimensional crystal structure. The conducting properties of other $M_4M'_{20}O_{62}$ (M = Sb, Bi; M' = Mo, W) phases are also discussed.

Introduction

Most molybdenum and tungsten oxides and bronzes (*1–9*) are low-dimensional metals and exhibit interesting physical properties. A remarkable feature is that some of these compounds are low-dimensional conductors despite their three-dimensional (3D) crystal structures. These systems are often structurally quite complex (*10*), and hence it is convenient to have some qualitative guidelines by which to single out what parts of their structures are responsible for their low-dimensional transport properties. These oxides and bronzes have extended networks of MO_6 (M = Mo, W) octahedra, and the average d-electron count on the transition metal atom is very low (i.e., between d^0 and d^1). Hence, only the lowest lying part of the t_{2g} block levels can be filled. Distortions of some of the MoO_6 octahedra lead to short M–O bond lengths, and thus some or all of their t_{2g} levels are raised in energy, thereby not contributing significantly to the lowest lying t_{2g} block bands. Consequently, a detailed analysis of the crystal structures of these materials provides important insight into what parts of their crystal structures control their transport properties (*9*).

$Sb_4M_{20}O_{62}$ is a semiconductor (*11*) with a complex 3D crystal structure (*12*). With respect to the structure of $Sb_4M_{20}O_{62}$, $Bi_4M_{20}O_{62}$ has a ($2a$, $2b$, $2c$) superstructure and is semiconducting (*13*). The tungsten analogs, $M_4W_{20}O_{62}$ (M = Sb, Bi), as well as some mixed molybdenum–tungsten bronzes, $M_4W_{20-x}Mo_xO_{62}$ (M = Sb, Bi), are also known (*14, 15*). All of them are semiconducting except for $Sb_4W_{20}O_{62}$, which is metallic (*14, 16*). Although the detailed crystal structure is known only for $Sb_4Mo_{20}O_{62}$ (*12*), all these phases possess the same basic structure (*14*). It is challenging to correlate

0022-4596/93 $5.00

the transport and structural properties of such structurally complex materials. In the present work, we examine how the semiconducting and metallic properties of these compounds are related to their crystal structures by performing extended Hückel tight binding (EHTB) electronic band structure calculations (*17*) for $Sb_4Mo_{20}O_{62}$. The structural and transport properties of low-dimensional oxides and bronzes have been successfully explained on the basis of EHTB calculations (*9*).

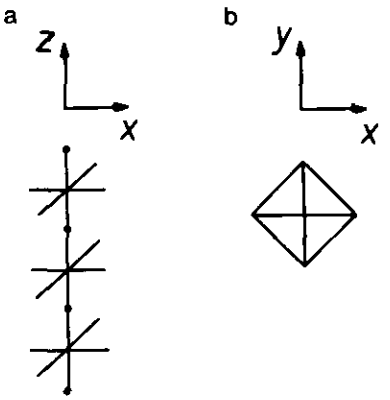

SCHEME 2

Crystal Structure

Shown in Scheme 1 is a top projection view of the quadruple chain unit Mo_4O_{16} obtained by sharing the corners of four MoO_5 single octahedral chains (Scheme 2). Corner sharing by these quadruple chains leads to Mo_4O_{14} slabs (Scheme 3). The Mo_5O_{15} 3D network (Scheme 4) of $Sb_4Mo_{20}O_{62}$ is obtained when the Mo_4O_{14} slabs (Scheme 3) are condensed with MoO_5 single octahedral chains (Scheme 2). The 3D network (Scheme 4) is the first member of the family of intergrowth tungsten bronzes characterized by Hussain and Kihlborg (*18*), and it can also be constructed from the condensation of Mo_5O_{19} quintuple chains (Scheme 5) (Fig. 1). The first member of the tetragonal tungsten bronze family can be described as a slightly different condensation of the units in Scheme 5 (*19*).

$Sb_4Mo_{20}O_{62}$ (see Fig. 1) contains Sb_2O units (···Sb–O–Sb···Sb–O–Sb···) inside the hexagonal channels of Scheme 4 in such a way that every Sb atom forms an SbO_3 trigonal pyramid. In addition, every MoO_6 octahedron shows a strong O–Mo···O bond alternation (i.e., of the order of 1.67 vs 2.35 Å) along the *b* axis. Every Mo atom of MoO_6 is located slightly out of the plane of the four equatorial O atoms, as depicted in Fig. 1, where the filled and empty circles represent the Mo atoms lying above and below this plane, respectively. The senses of the O–Mo···O alternation at the two kinds of Mo atoms are opposite (i.e., O–Mo···O at one and O···Mo–O at the other), so that the unit cell of Scheme 4 is given by $(Mo_5O_{15})_4$. Hence, $Sb_4Mo_{20}O_{62}$ can be formulated as $(Sb_2O)_2(Mo_5O_{15})_4$.

With the formal oxidation states of Sb^{3+} and O^{2-}, there are eight electrons to fill the t_{2g} block bands of the $Mo_{20}O_{60}$ 3D network

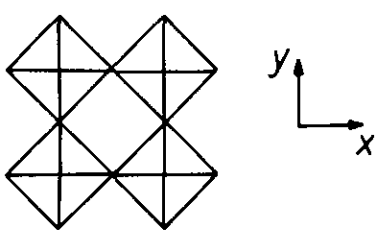

SCHEME 1

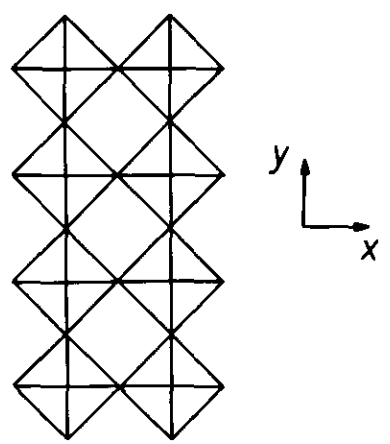

SCHEME 3

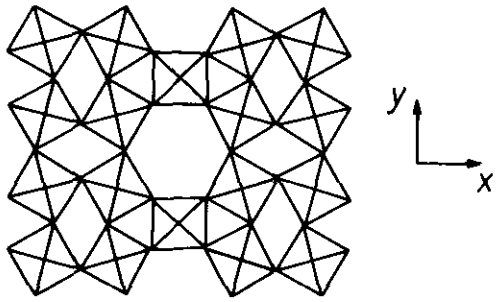

SCHEME 4

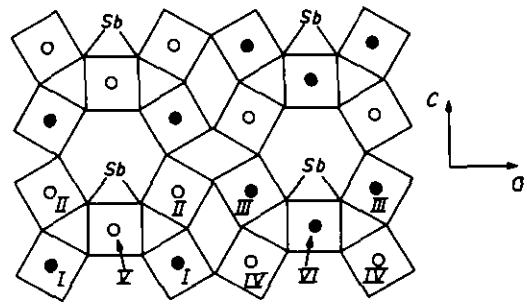

FIG. 1. Projection view of the crystal structure of $Sb_4Mo_{20}O_{62}$ along the b axis (*12*). The filled and empty circles denote Mo atoms above and below the planes of the four equatorial oxygen atoms, respectively.

(Scheme 4) of $Sb_4Mo_{20}O_{62}$. $Sb_4Mo_{20}O_{62}$ can be either a regular semiconductor (i.e., there is an energy gap between the fourth and the fifth t_{2g} block bands of the Mo_5O_{15} 3D network) or a Mott insulator. To distinguish between these two alternatives, it is necessary to consider how the distortions of the different MoO_6 octahedra control the nature of the low-lying t_{2g} block bands of the Mo_5O_{15} 3D network.

Electronic Structure

A. Octahedral distortion and low-lying t_{2g} levels. The t_{2g} block levels of a regular MoO_6 octahedron have antibonding combinations between the Mo *d* orbitals and the O *p* orbitals. Hence, a shortening of an Mo–O bond length raises the energy of any t_{2g} block orbital if it has an antibonding combination between the Mo and O orbitals along the shortened Mo–O bond. Consequently, a distortion where one Mo–O bond is shortened leaves one t_{2g} level (i.e., the one that is δ with respect to the shortened Mo–O bond) and raises the energy of the remaining two levels (Scheme 6). By contrast, all three t_{2g} levels are raised by a distortion in which two or more Mo–O bonds (in *cis* arrangement) are shortened (Scheme 6) (9).

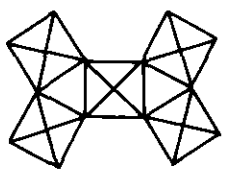

SCHEME 5

As mentioned, all MoO_6 octahedra in $Sb_4Mo_{20}O_{62}$ have a strong O–Mo···O alternation along the *b* direction. Consequently, only one t_{2g} level of any MoO_6 octahedra (i.e., the one contained in the *ac* plane, denoted as the equatorial plane hereafter) can contribute to the low-lying *d* block bands. Since these orbitals are of δ-type with respect to the *b* direction, the low-lying t_{2g} block bands should not be dispersive in that direction. Shown in Fig. 2 are the various basal Mo–O bond lengths found in $Sb_4Mo_{20}O_{62}$ (*12*). In addition to the strong alternation along the *b* direction, the $Mo^{(V)}O_6$ octahedra have two very short Mo–O bonds (1.72 Å) in the *ac* plane. Consequently, the three t_{2g} levels of the $Mo^{(V)}O_6$

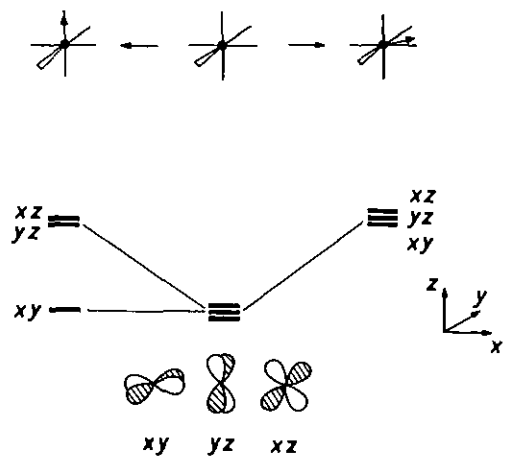

SCHEME 6

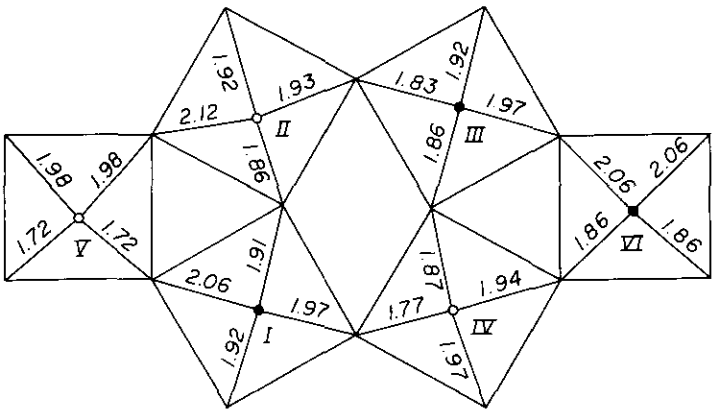

FIG. 2. Mo–O distances associated with the basal O atoms for the six different types of MoO_6 octahedra in $Sb_4Mo_{20}O_{62}$.

octahedra are very high in energy and do not participate in the low-lying t_{2g} block bands. As a consequence, these bands are not dispersive along the *a* direction either. As a result, $Sb_4Mo_{20}O_{62}$ is expected to be a good conductor only along the *c* direction.

B. Octahedral condensation and low-lying t_{2g} levels. The previous analysis suggests that five of the six different types of MoO_6 octahedra each contribute one t_{2g} orbital to the low-lying *d* block bands, and that $Sb_4Mo_{20}O_{62}$ should be a very anisotropic semiconductor. To understand the temperature dependence of the electrical conductivity of this compound, we need to consider the nature of its low-lying *d* block bands in more detail. Shown in Fig. 3 are the low-lying t_{2g} levels of the Mo_4O_{20} (Scheme 7) and Mo_9O_{42} (Scheme 8) clusters taken from the crystal structure of $Sb_4Mo_{20}O_{62}$. The four low-lying levels of the Mo_4O_{20} cluster, labeled (a)–(d) in Figure 3, are indeed built from the equatorial t_{2g} orbitals of the four octahedra and are schematically shown in Schemes 9a–9d, respectively. For simplicity, the *p* orbitals of the unshared oxygen atoms are not shown in Schemes 9a–9d, and the dots are used to indicate the absence of the *p* orbital contribution from the shared oxygen atoms. Every one of these four orbitals leads to a slightly split pair of orbitals

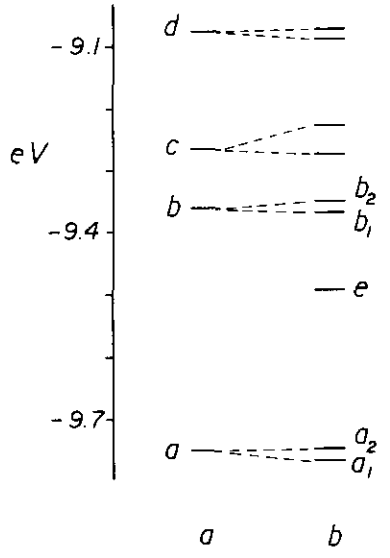

FIG. 3. Low-lying t_{2g} block levels of (a) Mo_4O_{20} and (b) Mo_9O_{42} clusters built from the crystal structure of $Sb_4Mo_{20}O_{62}$.

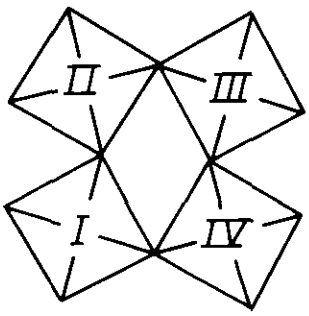

SCHEME 7

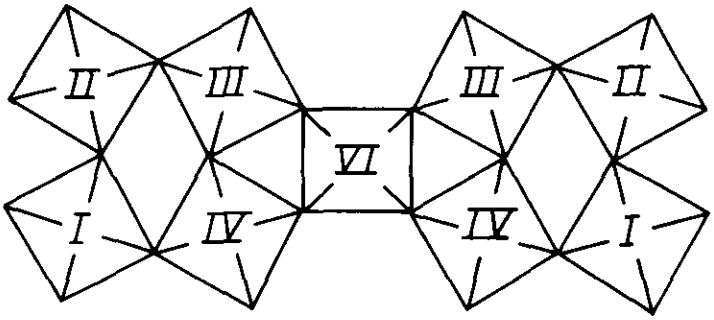

SCHEME 8

in the Mo_9O_{42} cluster (Fig. 3b). These pairs of levels are essentially the in-phase and out-of-phase combinations of the orbitals shown in Scheme 9a–9d with a very small contribution from the $Mo^{(V)}O_6$ octahedra. In addition, there is a new level, labeled e in Fig. 3b, between the two low-lying pairs of orbitals of the Mo_9O_{42} cluster. This level is essentially the equatorial t_{2g} level of the $Mo^{(VI)}O_6$ octahedron. The corresponding orbital of the $Mo^{(V)}O_6$ octahedron lies much higher in energy and is not shown in Fig. 3. The *a*-type levels of the Mo_4O_{20} and Mo_9O_{42} clusters are low in energy because the octahedral condensation decreases the antibonding contribution of the shared oxygen atoms. The condensation of the two Mo_4O_{20} clusters through the $Mo^{(VI)}O_6$ octahedra, with local 3-fold symmetry, does not significantly lower the energy of any of the (a)–(d) type

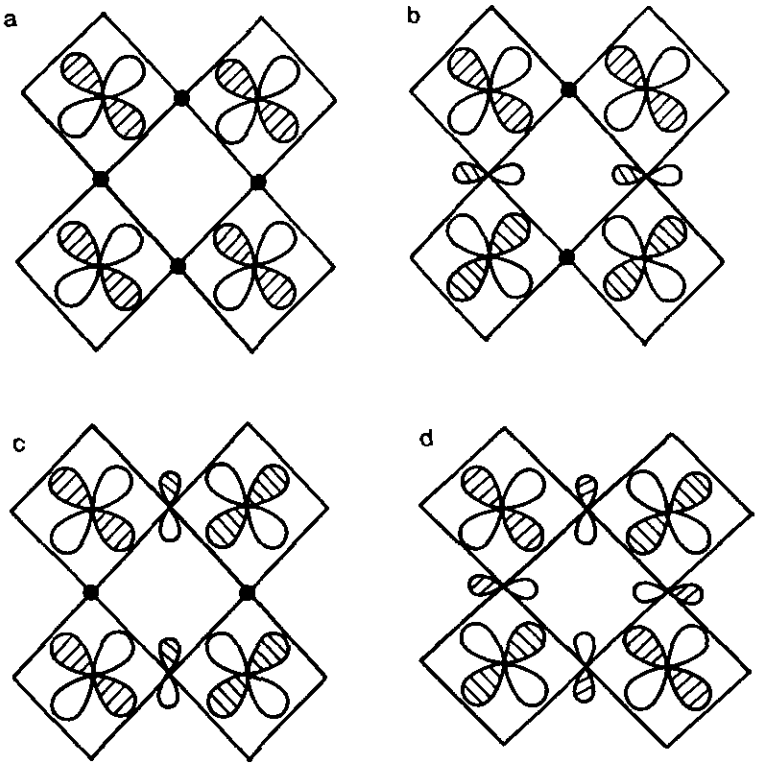

SCHEME 9

orbitals. This means that an octahedral condensation with local 3-fold symmetry is less effective than the one with local 4-fold symmetry (see later) in removing the antibonding contribution of the shared oxygen atoms.

C. Electronic band structure. The dispersion relations for the low-lying *d* block bands of $Sb_4Mo_{20}O_{62}$ are shown in Fig. 4. All bands appear in pairs of near degeneracy, because two $Mo_{10}O_{30}$ units repeat along the *b* direction due to the O–Mo···O bond alternation. The *d* orbitals associated with these bands are of δ-type along the *b* direction, thereby leading to pairs of nearly degenerate bands. The main orbital character of the bands labeled a_1, a_2, e, and b_1 is similar to that of the corresponding energy levels of the cluster in Scheme 8 (see Fig. 3). These bands are dispersionless along the *a* and *b* directions but show some dispersion along the *c* direction, in agreement with our structural analysis. The important result of Fig. 4 is that there is a band gap (E_g) of 0.22 eV between the fourth and fifth bands. This is compatible with the activation energy for the electrical conductivity of $Sb_4Mo_{20}O_{62}$ (E_a = 0.16 eV) (*11*), which suggests a band gap of 0.32 eV.

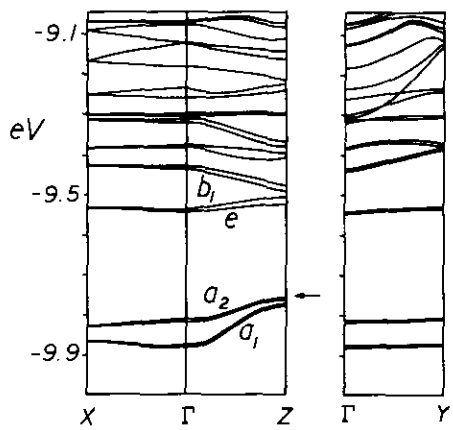

FIG. 4. Dispersion relations calculated for the low-ldying *d* block bands of $Sb_4Mo_{20}O_{62}$, where the arrow denotes the highest occupied level. Γ, *X*, *Y* and *Z* refer to (0, 0, 0), ($a^*/2$, 0, 0), (0, $b^*/2$, 0) and (0, 0, $c^*/2$, 0), respectively.

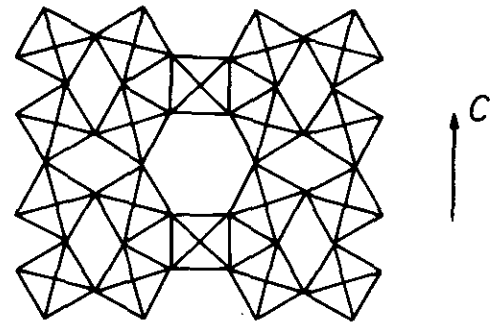

SCHEME 10

D. Structural origin of the band gap. The previous analysis suggests that as far as the conducting properties are concerned, $Sb_4Mo_{20}O_{62}$ can be considered as an assembly of noninteracting Mo_9O_{38} chains (Scheme 10) running along the *c* direction. Every chain of Scheme 10 consists of two Mo_4O_{18} chains (Scheme 11) weakly coupled through $Mo^{(VI)}O_6$ octahedra. The chain in Scheme 11 is also the structural fragment that is mainly responsible for the conducting properties of the blue bronzes $A_{0.3}MoO_3$ (*A* = K, Rb, Tl) and the red bronzes $A_{0.33}MoO_3$ (*A* = K, Rb, Cs, Tl) (*9*). However, the low-lying *d* block bands of the latter systems are much more dispersive. In order to understand the origin of the semiconducting properties of $Sb_4Mo_{20}O_{62}$, we need to consider why the low-lying t_{2g} block bands of the Mo_4O_{18} chains have a weak

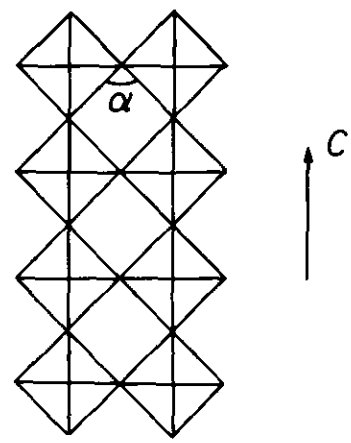

SCHEME 11

dispersion and are well separated from the low-lying t_{2g} levels of the bridging $Mo^{(VI)}O_6$ octahedra.

The angle α (see Scheme 11) for the real Mo_4O_{18} chain is far from 90° (Fig. 1). To study if such a rotation of the octahedra is responsible for the band gap, we calculate the band dispersion relations of an ideal Mo_4O_{18} chain (where the four basal Mo–O distances are 1.956 Å, i.e., the average of the experimental bond lengths in $Sb_4Mo_{20}O_{62}$, and the two axial Mo–O distances are 1.656 and 2.256 Å) for different values of the rotation angle α. Our results for $\alpha = 90°$ and $\alpha = 60°$ (close to the experimental value) are shown in Figs. 5a and 5b, respectively. The dispersion relations calculated for the real Mo_4O_{18} chain taken from $Sb_4Mo_{20}O_{62}$ are shown in Fig. 5c. The important results of Fig. 5 are as follows: (a) bands a and b at Z and band c at Γ are degenerate for the ideal chain with $\alpha = 90°$, (b) changing α from 90° to 60° reduces the bandwidths only slightly and keeps the above mentioned degeneracy, and (c) only in the real chain, bands c and d rise above band b, and the degeneracy at Z disappears. According to these results, it is not the rotation but the distortions of the MoO_6 octahedra that are responsible for the band gap in the real chain.

The main orbital components of bands a–d are those of the cluster orbitals in Schemes 9a–9d, respectively. Bands a and b at Z for the ideal chain with $\alpha = 90°$ have the nodal patterns in Schemes 12 and 13. Band c at Γ has the nodal pattern in Scheme 14. These band levels are degenerate because they have the same number of antibonding oxygen p orbital contributions (i.e., two per unit cell). Bands a and b are no longer degenerate in the real chain because, as shown in Fig. 2, there is an O···Mo–O–Mo···O alternation along the c direction. Since the short distances are associated with the local 4-fold octahedral condensation, the lower energy orbital (i.e., band a at Z) is given by Scheme 12. (The 4-fold condensation occurs between the dashed lines.) The real chain also has an O···Mo–O–Mo···O alternation of bonds in the direction perpendicular to the c axis (see Fig. 2). Since band c at Γ is given by Scheme 14 and since the short Mo–O distances perpendicular to the c axis are shorter than the long Mo···O distances along the c axis, band

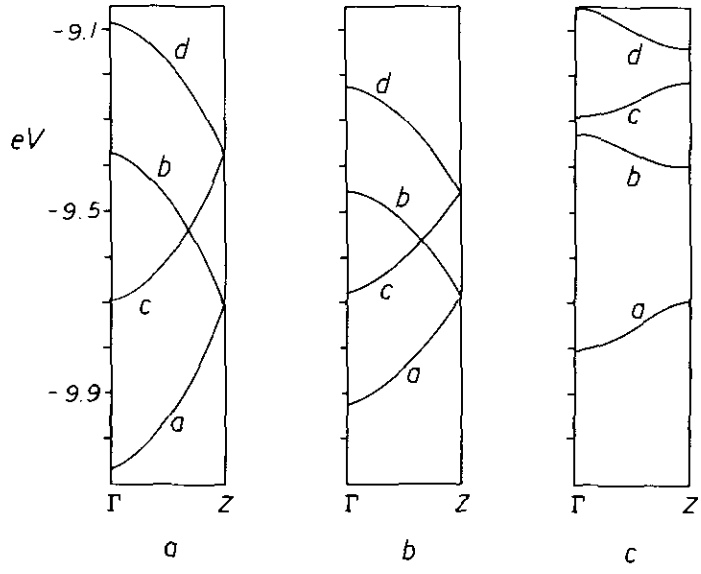

FIG. 5. Dispersion relations calculated for a Mo_4O_{18} chain with strong axial O–Mo···O alternation: (a) for an ideal chain with $\alpha = 90°$, (b) for an ideal chain with $\alpha = 60°$, and (c) for the real chain found in $Sb_4Mo_{20}O_{62}$.

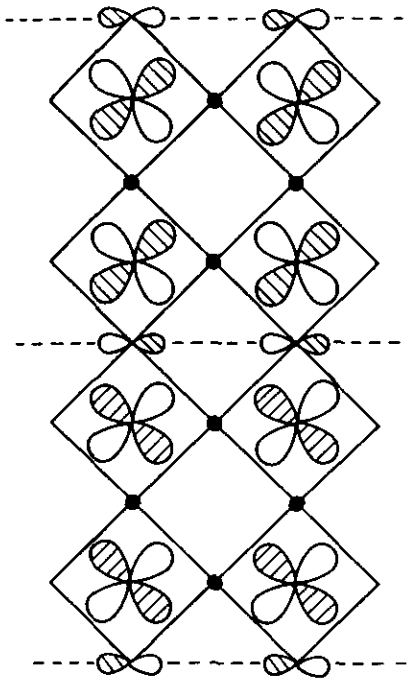

SCHEME 12

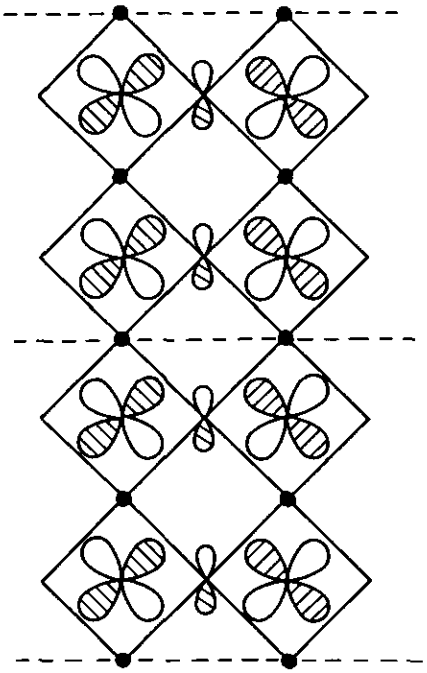

SCHEME 14

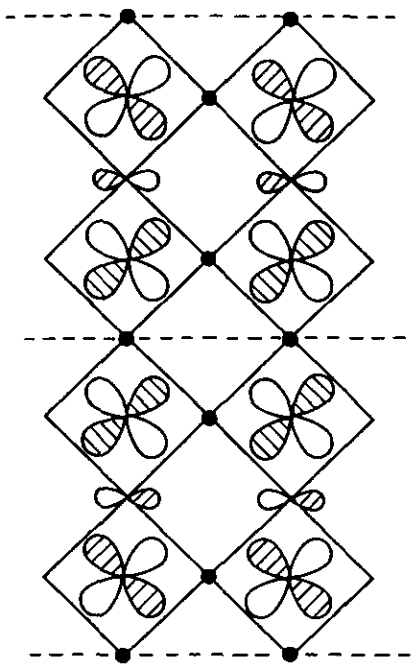

SCHEME 13

c at Γ is far above band a at Z. The final question to consider is why band e is closest to band b at Z, thereby keeping a band gap for 3D $Sb_4Mo_{20}O_{62}$. The nodal pattern of band b at Z is given by Scheme 13, while band e is mainly built from the basal t_{2g} orbital of the $Mo^{(VI)}O_6$ octahedra. As shown in Fig. 2, the short Mo–O distances along the c direction and the two short Mo–O distances of the $Mo^{(VI)}O_6$ octahedra are practically identical. Thus bands b and e should be similar in energy. Consequently, there occurs a band gap at the Fermi level of $Sb_4Mo_{20}O_{62}$.

E. Conducting Properties of $M_4M'_{20}O_{62}$ phases (M = Sb, Bi; M' = Mo, W). Our calculations clearly demonstrate that $Sb_4Mo_{20}O_{62}$ is a regular semiconductor. The $Bi_4Mo_{20}O_{62}$ phase has a ($2a$, $2b$, $2c$) superstructure of the $Sb_4Mo_{20}O_{62}$ structure. This superstructure is most likely related to a slightly more complex arrangement of the Bi_2O units inside the hexagonal channels and is not expected to modify the octahedral

network in any substantial way. Hence both phases should be regular semiconductors with very similar band gaps E_g. This is in agreement with the values of E_g derived from conductivity measurements (0.32 (*11*) and 0.36 (*13*) eV for $Sb_4Mo_{20}O_{62}$ and $Bi_4Mo_{20}O_{62}$, respectively). The WO_6 octahedra commonly found in tungsten oxides and bronzes usually do not have strong O–W···O alternations. Although the detailed crystal structures of the $M_4W_{20}O_{62}$ (M = Sb, Bi) phases are not known, it is very likely that there will not be strong O–W···O alternations along the b axis. The pattern of distortions in the ac plane can be somewhat reduced but will probably remain, since it results from the strain generated by the local 3-fold octahedral condensation and the need to accommodate the M_2O (M = Sb, Bi) units in the channels. The weakly distorted nature of the WO_6 octahedra leads to a very small splitting of the t_{2g} orbitals (*20*). In the absence of strong alternations along the axial direction of the octahedra, π-type interactions that occur along this direction among the π-type t_{2g} orbitals lead to strongly dispersive bands. The resulting dispersive bands may cross the less dispersive bands resulting from the δ-type t_{2g} orbitals, thereby leading to partially filled bands and hence metallic conductivity (*21*). We believe this situation applies for $Sb_4W_{20}O_{62}$ and accounts for its metallic conductivity. The structure of $Bi_4W_{20}O_{62}$ could not be solved using the ($2a$, $2b$, $2c$) superstructure of $Bi_4Mo_{20}O_{62}$, which suggests a disorder in the arrangement of the Bi_2O units in the hexagonal channels. Such a disorder introduces a random potential and can destroy the metallic conductivity of this phase. The same type of disorder-induced localization should apply for the mixed phases $M_4W_{20-x}Mo_xO_{62}$ (M = Sb, Bi).

Concluding Remarks

Our calculations show that $Sb_4Mo_{20}O_{62}$ has a band gap at the Fermi level, and thus it is a regular semiconductor, not a Mott insulator. A similar situation was found for the molybdenum red bronzes $A_{0.33}MoO_3$ (A = Li, K, Cs and Tl) (*22*). Despite its 3D crystal structure, $Sb_4Mo_{20}O_{62}$ is calculated to be a one-dimensional semiconductor. Analysis of the low-lying d block band orbitals shows that this band gap originates from the O–Mo···O alternation in the six different types of MoO_6 octahedra. To understand the conducting properties of the tungsten analogs, one should take into consideration both the smaller extent of distortion in the WO_6 octahedra and the random potentials arising from a random arrangement of the Bi_2O units.

Acknowledgments

This work was supported by the U.S. Department of Energy, Office of Basic Sciences, Division of Materials Science, under Grant DE-FG05-86ER45259; by NATO, Scientific Affairs Division, under Grant CRG 910129; and by the Centre National de la Recherche Scientifique, France.

References

1. C. Schlenker, J. Dumas, C. Escribe-Filippini, and H. Guyot, *in* "Low-Dimensional Electronic Properties of Molybdenum Bronzes and Oxides" (C. Schlenker, Ed.), p. 159, Kluwer, Dordrecht (1989).
2. C. Schlenker, J. Dumas, C. Escribe-Filippini, H. Guyot, J. Marcus, and J. Fourcadot, *Philos. Mag. B* **52,** 643 (1985).
3. J. P. Pouget, *in* "Low-Dimensional Electronic Properties of Molybdenum Bronzes and Oxides" (C. Schlenker, Ed.) p. 87, Kluwer, Dordrecht (1989).
4. M. Greenblatt, *in* "Low-Dimensional Electronic Properties of Molybdenum Bronzes and Oxides" (C. Schlenker, Ed.) p. 1, Kluwer, Dordrecht (1989).
5. M. Greenblatt, *Chem. Rev.* **88,** 31 (1988).
6. R. M. Fleming and R. Cava, *in* "Low-Dimensional Electronic Properties of Molybdenum Bronzes and Oxides" (C. Schlenker, Ed.), p. 259, Kluwer, Dordrecht (1989).
7. (a) E. Wang, M. Greenblatt, I. E.-I. Rachidi, E. Canadell, M.-H. Whangbo, and S. Vadlamannati, *Phys. Rev B* **39,** 12969 (1989); (b) E. Wang, M. Greenblatt, I. E.-I. Rachidi, E. Canadell, and M.-J. Whangbo, *J. Solid State Chem.* **81,** 173 (1989); (c) E. Wang, M.

GREENBLATT, I. E.-I. RACHIDI, E. CANADELL, AND M.-H. WHANGBO, *J. Solid State Chem.* **80,** 266 (1989); (d) P. FOURY, J. P. POUGET, E. WANG, AND M. GREENBLATT, *Europhys. Lett.* **16,** 485 (1991); (e) P. FOURY, J. P. POUGET, Z. S. TEWELDEMEDHIN, AND M. GREENBLATT, *Synth. Met.*, in press.

8. M.-H. WHANGBO, E. CANADELL, P. FOURY, AND J. P. POUGET, *Science* **252,** 96 (1991).
9. (a) E. CANADELL AND M.-H. WHANGBO, *Chem. Rev.* **91,** 965 (1991); (b) M.-H. WHANGBO AND E. CANADELL, *Acc. Chem. Res.* **22,** 375 (1989).
10. (a) H. VINCENT, AND M. MAREZIO, *in* "Low-Dimensional Electronic Properties of Molybdenum Bronzes and Oxides" (C. Schlenker, Ed.), p. 49, Kluwer, Dordrecht, (1989); (b) L. KIHLBORG, *Arkiv. Kemi* **21,** 471 (1963); (c) B. RAVEAU, *Proc. Indian Nat. Sci. Acad. A* **52,** 67 (1986).
11. A. BONNET, A. CONAN, H. QUEINNEC, M. GANNE, AND M. DION, *Phys. Rev. B* **30,** 688 (1984).
12. M. PARMENTIER, C. GLEITZER, A. COURTOIS, AND J. PROTAS, *Acta Crystallogr. Sect. B* **35,** 1963 (1979).
13. A. CONAN, A. BONNET, M. GANNE, AND M. DION, *J. Phys. Chem. Solids* **46,** 721 (1985).
14. M. TOURNOUX, M. GANNE, AND Y. PIFFARD, *J. Solid State Chem.* **96,** 141 (1992).
15. M. DION, Ph.D. Thesis, Nantes (1984).
16. A. BONNET, A. CONAN, M. MORSLI, M. GANNE, AND M. TOURNOUX, *Phys. Satus. Solidi B* **150,** 225 (1988).
17. M.-H. WHANGBO AND R. HOFFMANN, *J. Am. Chem. Soc.* **100,** 6093 (1988). Our calculations are of the extended Hückel type (R. HOFFMANN, *J. Chem. Phys.* **39,** 1397 (1963)) with exponents and parameters taken from previous work (M.-H. WHANGBO AND L. F. SCHNEEMEYER, *Inorg. Chem.* **25,** 2425 (1986); T. HUGHBANKS, R. HOFFMANN, M.-H. WHANGBO, K. R. STEWART, O. EISENSTEIN, AND E. CANADELL, *J. Am. Chem. Soc.* **104,** 3876 (1982)). A modified Wolfsberg–Helmholz formula (J. AMMETER, H.-B. BÜRGI, J. THIBEAULT, AND R. HOFFMANN, *J. Am. Chem. Soc.* **100,** 3686 (1978)) was used to evaluate the off-diagonal $H_{\mu\nu}$ values.
18. A. HUSSAIN AND L. KIHLBORG, *Acta Crystallogr. Sect. A* **32,** 551 (1976).
19. M. GANNE, M. DION, A. VERBAERE, AND M. TOURNOUX, *J. Solid State Chem.* **29,** 9 (1979).
20. E. CANADELL, M.-H. WHANGBO AND I. E.-I. RACHIDI, *Inorg. Chem.* **29,** 3871 (1990).
21. (a) M.-H. WHANGBO AND E. CANADELL, to be published; (b) J. D. MARTIN AND E. CANADELL, to be published.
22. (a) M.-H. WHANGBO, M. EVAIN, E. CANADELL, AND M. GANNE, *Inorg. Chem.* **28,** 267 (1989); (b) E. CANADELL AND M.-H. WHANGBO, *Inorg. Chem.* **28,** 1609 (1989).